© 2017. Published by The Company of Biologists Ltd | Journal of Cell Science (2017) 130, 2757-2766 doi:10.1242/jcs.205369

TOOLS AND RESOURCES

An improved Akt reporter reveals intra- and inter-cellular heterogeneity and oscillations in signal transduction

Dougall M. Norris[1,*], Pengyi Yang[2,*], James R. Krycer[1], Daniel J. Fazakerley[1], David E. James[1,3] and James G. Burchfield[1,‡]

ABSTRACT

Akt is a key node in a range of signal transduction cascades and play a critical role in diseases such as cancer and diabetes. Fluorescently-tagged Akt reporters have been used to discern Akt localisation, yet it has not been clear how well these tools recapitulate the behaviour of endogenous Akt proteins. Here, we observed that fusion of eGFP to Akt2 impaired both its insulin-stimulated plasma membrane recruitment and its phosphorylation. Endogenous-like responses were restored by replacing eGFP with TagRFP-T. The improved response magnitude and sensitivity afforded by TagRFP-T–Akt2 over eGFP–Akt2 enabled monitoring of signalling outcomes in single cells at physiological doses of insulin with subcellular resolution and revealed two previously unreported features of Akt biology. In 3T3-L1 adipocytes, stimulation with insulin resulted in recruitment of Akt2 to the plasma membrane in a polarised fashion. Additionally, we observed oscillations in plasma membrane localised Akt2 in the presence of insulin with a consistent periodicity of 2 min. Our studies highlight the importance of fluorophore choice when generating reporter constructs and shed light on new Akt signalling responses that may encode complex signalling information.

This article has an associated First Person interview with the first author of the paper.

KEY WORDS: Akt, Recruitment, Oscillation, Adipocyte, Insulin, Signalling

INTRODUCTION

Imaging of signal transduction in live single cells is essential for achieving both the spatial and temporal resolution required for dissecting complex patterns of information that can be encoded within signals (Kurakin, 2005; Sonnen and Aulehla, 2014). The success of the live-cell imaging approach is reliant on stable, sensitive reporter constructs that recapitulate the behaviour of their endogenous surrogates as faithfully as possible. To achieve this, careful design of the reporter is essential, and genetically encoded reporters need to be carefully validated. In particular, it is becoming increasingly clear that choice of fluorophore is critical in obtaining optimal functionality. Here, we describe an improved reporter for Akt and demonstrate that eGFP tagging of Akt2 impairs its biological function.

The Ser/Thr kinase Akt proteins serve as a master signalling switch (Manning and Cantley, 2007), whose recruitment to the plasma membrane (PM) and subsequent activation is essential for many distinct cellular processes including metabolism, cell growth, survival and apoptosis (Kandel and Hay, 1999). There are three Akt isoforms (Akt1, Akt and Akt3; hereafter generically referred to as Akt) that have distinct tissue distribution profiles and reportedly distinct functions (Dummler and Hemmings, 2007). Akt possesses an N-terminal pleckstrin homology (PH) domain, a kinase domain and a C-terminal hydrophobic motif. The PH domain has a high affinity for phosphatidylinositol (3,4,5)-triphosphate (PIP3), a phospholipid that is produced by PI3 kinase (PI3K) in response to growth factor stimulation and is degraded by phosphatase and tensin homolog (PTEN) and SH2 domain containing inositol 5-phosphatase 2 (SHIP2, also known as INPPL1). Recruitment of Akt to the PM via its PH domain is critical for its activation. The PH-domain–PIP3 interaction is thought to cause a conformational change that allows Akt to be activated by phosphorylation on Thr309 (in Akt2; T308 in Akt1, T305 in Akt3) and Ser474 (in Akt2; S473 in Akt1, S472 in Akt3) residues by the kinases PDK1 (also known as PDPK1) and mTORC2, respectively (Alessi et al., 1997; Sarbassov, 2005).

Subcellular fractionation and immunofluorescence imaging of endogenous Akt suggest that it is strongly recruited to the PM in response to growth factor stimulation (Carvalho et al., 2000; Currie et al., 1999; Wang, 2006). Furthermore, live-cell imaging of fluorescent Akt reporter constructs have revealed important insights such as isoform specificity, chemotaxis, phospholipid binding, conformational changes in Akt, nuclear activation and membrane diffusion rates, across a range of cell lines (Calleja et al., 2003; Gonzalez and McGraw, 2009; Kontos et al., 1998; Lasserre et al., 2008; Servant et al., 2000; Wang and Brattain, 2006). Numerous groups have assessed Akt recruitment to the PM in response to various stimuli in live cells by using GFP-tagged full-length Akt and Akt PH domain constructs. The extent of Akt membrane recruitment in these studies was highly variable. Furthermore, none of these studies appear to have compared the activity and/or function of these constructs to the endogenous protein (Asano et al., 2008; Calleja et al., 2003; Carpten et al., 2007; Cenni et al., 2003; Currie et al., 1999; Du et al., 2014; Feng et al., 2014; Gonzalez and McGraw, 2009; Huang et al., 2011; Imazaki et al., 2010; Kontos et al., 1998; Lasserre et al., 2008; Parikh et al., 2012; Rodríguez-Escudero et al., 2005; Servant et al., 2000; Terashima et al., 2005; Watton and Downward, 1999; Zhang et al., 2009). While GFP remains the most commonly used fluorescent protein, there are a growing number of publications that report fusion protein dysfunction (Goto et al., 2003; Huang and Shusta, 2006;

[1]Charles Perkins Centre, School of Life and Environmental Sciences, The University of Sydney, Sydney, NSW 2006, Australia. [2]Charles Perkins Centre, School of Mathematics and Statistics, The University of Sydney, Sydney, NSW 2006, Australia. [3]Sydney Medical School, The University of Sydney, Sydney, NSW 2006, Australia.
*These authors contributed equally to this work

‡Author for correspondence (james.burchfield@sydney.edu.au)

D.M.N., 0000-0001-8201-4999; P.Y., 0000-0003-1098-3138; J.R.K., 0000-0003-1536-7270; D.J.F., 0000-0001-8241-2903; D.E.J., 0000-0001-5946-5257; J.G.B., 0000-0002-6609-6151

Received 21 April 2017; Accepted 26 June 2017

Journal of Cell Science

Journal of Cell Science (2017) 130, 2757-2766 doi:10.1242/jcs.205369

Kalatskaya et al., 2006; Liu et al., 1999; Yantsevich et al., 2009) and mislocalisation (Skube et al., 2010; Zhu et al., 2013), which one group has attributed to the affinity of eGFP for the nucleus (Seibel et al., 2007). Cellular stress responses have also been reported in cultured cells stably expressing GFP (Zhang et al., 2003), and eGFP expression has also been reported to increase production of superoxide and hydrogen peroxide (Ganini et al., 2017). Adverse effects have also been observed in transgenic GFP animals (Devgan et al., 2004; Huang et al., 2000; Mawhinney and Staveley, 2011). Therefore, despite GFP tagging of proteins driving huge advances in our understanding of biological processes, GFP is not as inert as previously assumed.

Here, we report that eGFP–Akt2 exhibits impaired insulin-regulated recruitment and phosphorylation when compared to the endogenous protein. With the availability of brighter, more photostable fluorophores that have a reduced propensity to oligomerise (Cranfill et al., 2016) and have distinct structural features (e.g. electrostatic charge), we wished to determine whether an alternate fluorophore may allow us to develop a more accurate Akt reporter. Indeed, we observed a markedly enhanced response in both recruitment and phosphorylation of Akt2 when fused to TagRFP-T (Shaner et al., 2008) compared to eGFP-tagged Akt2. The improved dynamics of this reporter enabled us to detect intricacies of Akt2 recruitment to the PM, including oscillations at the cell surface, which could be important with regard to complex information transmission.

RESULTS

TagRFP-T–Akt2, but not eGFP–Akt2, is recruited to the PM in a similar manner to endogenous Akt

In order to study Akt in live cells, it is vital to have Akt reporter constructs that recapitulate the responses of endogenous Akt. The first step in Akt activation is the PIP3-dependent recruitment of Akt to the PM (Ng et al., 2008). We assessed the localisation of endogenous Akt (pan-Akt antibody) in 3T3-L1 adipocytes by performing immunofluorescence confocal microscopy (Fig. 1A). Under basal conditions, Akt displayed diffuse cytoplasmic staining and clear nuclear localisation. Insulin resulted in decreased cytosolic staining and the appearance of a strong ‘rim’ signal at the cell periphery, characteristic of accumulation at the PM.

Similar to endogenous Akt, eGFP–Akt2 exhibited cytoplasmic and nuclear localisation under basal conditions when expressed in 3T3-L1 adipocytes (Fig. 1B–D). However, in contrast to endogenous Akt, eGFP–Akt2 displayed poor membrane redistribution in response to insulin (Fig. 1B–D). We hypothesised that poor recruitment of eGFP–Akt was an artefact of eGFP tagging and that recruitment could be improved through the use of an alternate fluorophore. In particular, eGFP has a highly negative electrostatic charge (Fig. S1B). Since Akt PM recruitment is dependent on binding of the positively charged PH domain (Fig. S1C) to the negatively charged PIP3 (Levental et al., 2008), it may be that electrostatic repulsion between eGFP and PIP3 impairs this process or that electrostatic attraction between eGFP and the PH domain may sterically interfere with the PH domain. TagRFP-T has a relatively even surface charge distribution and has no net electrostatic charge (Fig. S1D) despite high structural similarity to eGFP (Fig. S1E). Furthermore, the brightness, photostability, rapid maturation and distinct origin (*Entacmaea quadricolor* versus *Aequorea victoria*) of TagRFP-T made it an ideal alternative to eGFP. TagRFP-T–Akt2 was expressed in 3T3-L1 adipocytes at similar levels to eGFP–Akt2 and localised similarly in unstimulated cells (Fig. 1B–D). However, stimulation of TagRFP-T–Akt2 with insulin resulted in a substantial redistribution to the periphery of the cell (Fig. 1B–D) in a similar manner to endogenous Akt (Fig. 1A).

TagRFP-T–Akt2 is highly insulin responsive in comparison to eGFP–Akt2

We next examined the translocation kinetics of the eGFP- and TagRFP-T-tagged Akt2 constructs in response to insulin by performing total internal reflection fluorescence (TIRF) microscopy. eGFP alone was used as a control and displayed no detectable change in localisation upon stimulation with insulin (Fig. 1B,C,E,F). We also assessed TagRFP-T alone under these conditions, and observed no insulin-stimulated change in localisation (Fig. 1B,C). Insulin stimulation increased the TIRF signal for both eGFP– and TagRFP-T–Akt2 (Fig. 1E–G), and both constructs displayed a graded intracellular dose response to insulin. However, TagRFP-T–Akt2 displayed significantly greater recruitment compared to eGFP–Akt2, with a more than 4.5-fold and 5.8-fold increase in PM levels in response to insulin at doses of 1 and 100 nM, respectively (Fig. 1F). The shape of the curves also differed, with the TagRFP-T fusion construct revealing an overshoot in PM recruitment following a 1 nM insulin stimulus (Fig. 1F, inset). This response was not evident in cells expressing the eGFP–Akt2 construct. Furthermore, substantial heterogeneity in TagRFP-T–Akt2 recruitment was observed between single cells exposed to the same dose of insulin, which was not as apparent with the eGFP–Akt2 construct (Fig. 1G).

TagRFP-T–Akt2 is highly phosphorylated in response to insulin

Following PM recruitment, Akt2 is phosphorylated at Thr309 by PDK1 and Ser474 by mTORC2. To further assess how well the Akt reporter constructs recapitulated the behaviour of endogenous Akt, we assessed insulin-stimulated phosphorylation of endogenous Akt, eGFP-Akt2 and TagRFP-T-Akt2 by western blotting with phosphospecific antibodies to phosphorylated (p)Thr309 and pSer474 (Fig. 2A). In addition, we assessed Akt activity by blotting for phosphorylation of the Akt-regulated phosphosite Thr642 in TBC1D4 (also known and hereafter referred to as AS160). Stimulation of adipocytes with 1 and 100 nM insulin dose dependently increased phosphorylation of endogenous Akt at Thr309 and Ser474 (Fig. 2B), and of AS160 Thr642 (Fig. 2C). Overexpression of TagRFP-T–Akt2 or eGFP–Akt2 had no effect on the phosphorylation of endogenous Akt at either Thr309 or Ser474 (Fig. 2B). There were no significant changes in phosphorylation of AS160 Thr642 with overexpression of either fluorescent Akt construct (Fig. 2C). This is not surprising given that only a small amount of active Akt is required for AS160 to be completely phosphorylated (Tan et al. 2012; Hoehn et al. 2008) and this is easily satisfied by endogenous Akt under these conditions.

Consistent with data on insulin-stimulated translocation to the PM (Fig. 1B–G), TagRFP-T–Akt2 was phosphorylated at both sites to a greater extent than eGFP–Akt2 in response to both 1 nM and 100 nM insulin. For example, at 100 nM insulin TagRFP-T–Akt2 was phosphorylated 14-fold and 9-fold more than eGFP–Akt2 at the Thr309 (Fig. 2D) and Ser474 (Fig. 2E) sites, respectively. Like endogenous Akt, TagRFP-T–Akt2 displayed a dose response from 1 nM to 100 nM. Taken together, analysis of translocation and phosphorylation suggests that activation of the eGFP–Akt2 fusion construct is impaired in comparison to activation of endogenous Akt. In contrast, the new TagRFP-T–Akt2 reporter more faithfully recapitulated the behaviour of endogenous Akt.

Journal of Cell Science (2017) 130, 2757-2766 doi:10.1242/jcs.205369

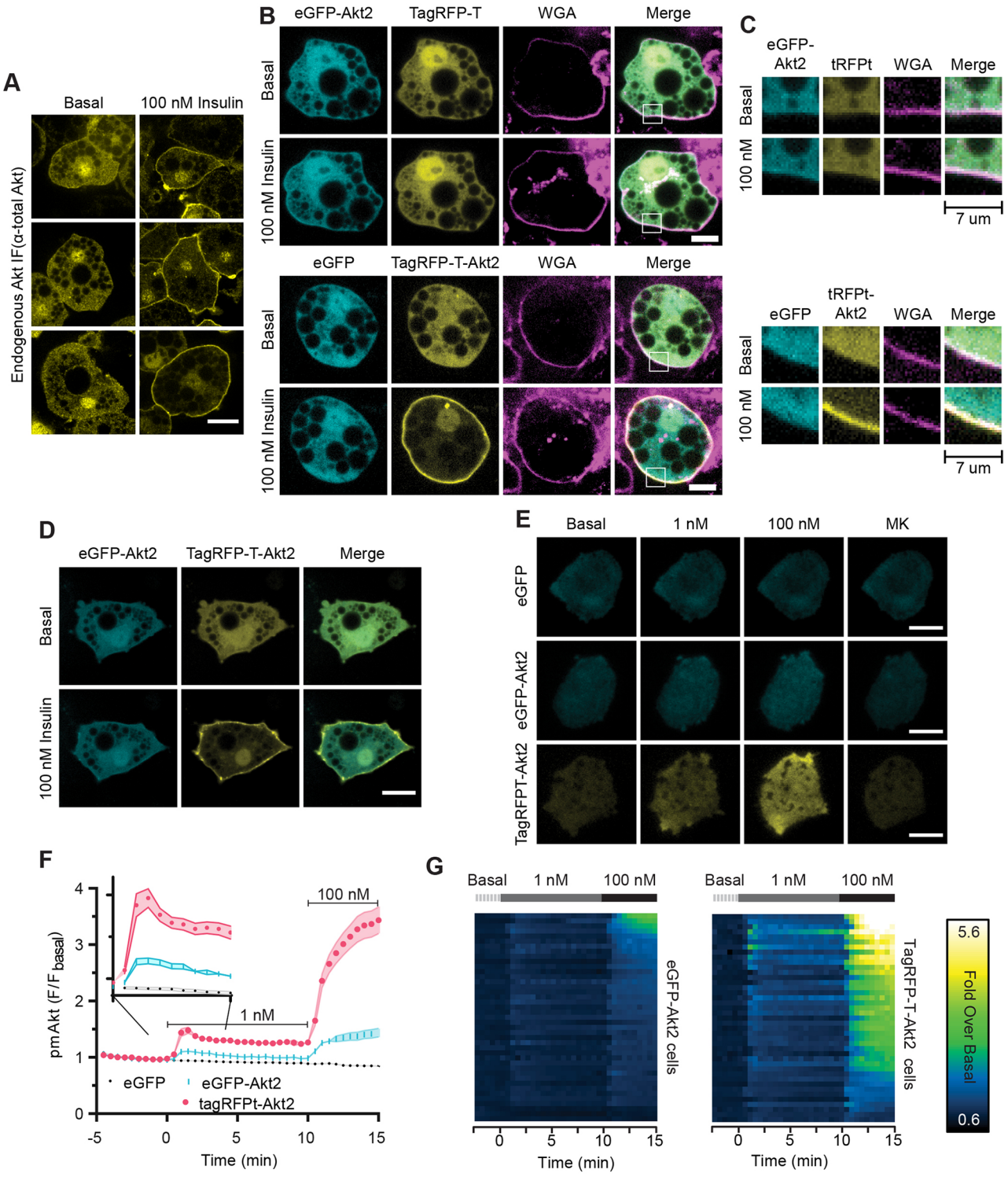

Fig. 1. TagRFP-T–Akt2, but not eGFP–Akt2, is highly insulin responsive and recruited to the PM in a similar manner to endogenous Akt. (A) Confocal immunofluorescence (IF) images of endogenous Akt (pan-Akt antibody) in 3T3-L1 adipocytes in the absence and presence of 100 nM insulin. (B) Confocal images of adipocytes co-expressing eGFP–Akt2 and TagRFP-T (upper panels), and adipocytes co-expressing TagRFP-T–Akt2 and eGFP (lower panels) in the presence and absence of 100 nM insulin. The fluorescent proteins TagRFP-T and eGFP were expressed as markers for the cytoplasm. Alexa Fluor 647-labelled wheat germ agglutinin (WGA) was added 6 min before the insulin stimulus and was used as a plasma membrane marker. (C) Enlarged regions of interest (white boxes in panel B) demonstrate the extent of colocalisation of each Akt construct with the cytoplasm or plasma membrane. The images are 7×7 µm. (D) Representative images of eGFP–Akt2 and TagRFP-T–Akt2 co-expression in a 3T3-L1 adipocyte imaged before and after stimulation (10 min) with 100 nM insulin taken with spinning disk microscopy. (E) Representative images displaying the recruitment of eGFP alone, eGFP–Akt2 and TagRFP-T–Akt2 into the TIRF zone in response to 1 and 100 nM insulin and after inhibition with MK2206 (MK). (F) Quantification of TIRF responses from 3T3-L1 adipocytes expressing eGFP, eGFP–Akt2 and TagRFP-T–Akt2 (n=27, 41 and 41 cells, respectively). Data are expressed as the mean (±s.e.m. indicated by shading). (G) Heatmap of the recruitment response for cells (as in F) expressing either eGFP–Akt2 or TagRFP-T–Akt2. Each row represents an average TIRF fluorescence for an single cell normalised to its basal fluorescence. Scale bars: 10 µm (A,B); 20 µm (D,E).

Journal of Cell Science

Journal of Cell Science (2017) 130, 2757-2766 doi:10.1242/jcs.205369

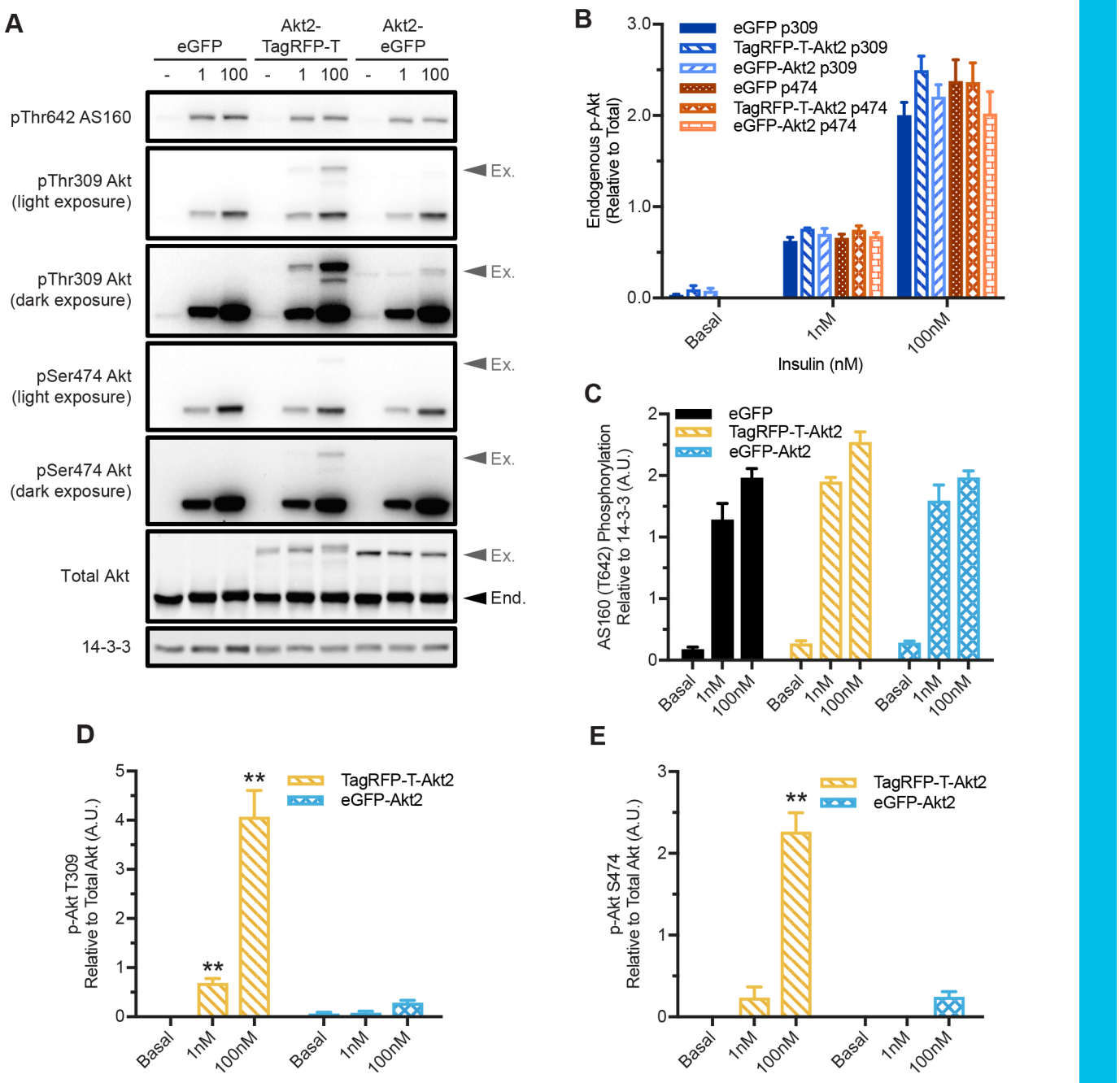

Fig. 2. TagRFP-T–Akt2, but not eGFP–Akt2, is highly phosphorylated in response to insulin. 3T3-L1 adipocytes expressing eGFP, eGFP–Akt2 or TagRFP-T–Akt2 were stimulated with 1 or 100 nM insulin for 10 min. (A) Representative western blot analysis of adipocyte lysates (n=3). The upper bands in the phosphorylated and total Akt blots are the exogenous Akt fluorescent fusion constructs (Ex.), which run at ~85 kDa. The lower bands are endogenous Akt (End.), which runs at ~60 kDa. (B–E) Densitometry analysis (in arbitrary units, A.U.) of blots shown in A. Quantification of endogenous Akt phosphorylation (B) and AS160 phosphorylation (C) from cells overexpressing the Akt2 fusion constructs. Quantification of eGFP–Akt2 and TagRFP-T–Akt2 phosphorylation at sites Thr309 (D) and Ser474 (E). Data are presented as mean±s.e.m. **P<0.01 compared with the eGFP–Akt2 equivalent (Student's t-test).

Insulin stimulates polarised Akt2 recruitment to the PM

The enhanced sensitivity of TagRFP-T–Akt2 permitted detection of subtle changes in the subcellular membrane association of Akt2 in response to insulin that was not apparent with eGFP–Akt2. These included polarised recruitment of Akt2 to the PM and oscillations in PM Akt2 that had a highly reproducible frequency.

TagRFP-T–Akt2 accumulated on the basal surface of 3T3-L1 adipocytes in response to insulin (Fig. 3A). Subsequently, membrane localisation of TagRFP-T–Akt2 became increasingly heterogeneous and Akt2 accumulated more intensely at the periphery of the basal surface (Fig. 3B–D). This was often accompanied by a decrease in signal at the centre of the cell (Fig. 3B–D). To define this behaviour more comprehensively, we expressed the fluorescence of individual pixels as a function of time and classified all pixels in a single cell using self-organising maps (SOMs). This analysis is presented such that regions exhibiting the same pattern of Akt2 translocation behaviour in response to insulin are given the same colour (Fig. 3E; Figs S2 and S3).

Journal of Cell Science (2017) 130, 2757-2766 doi:10.1242/jcs.205369

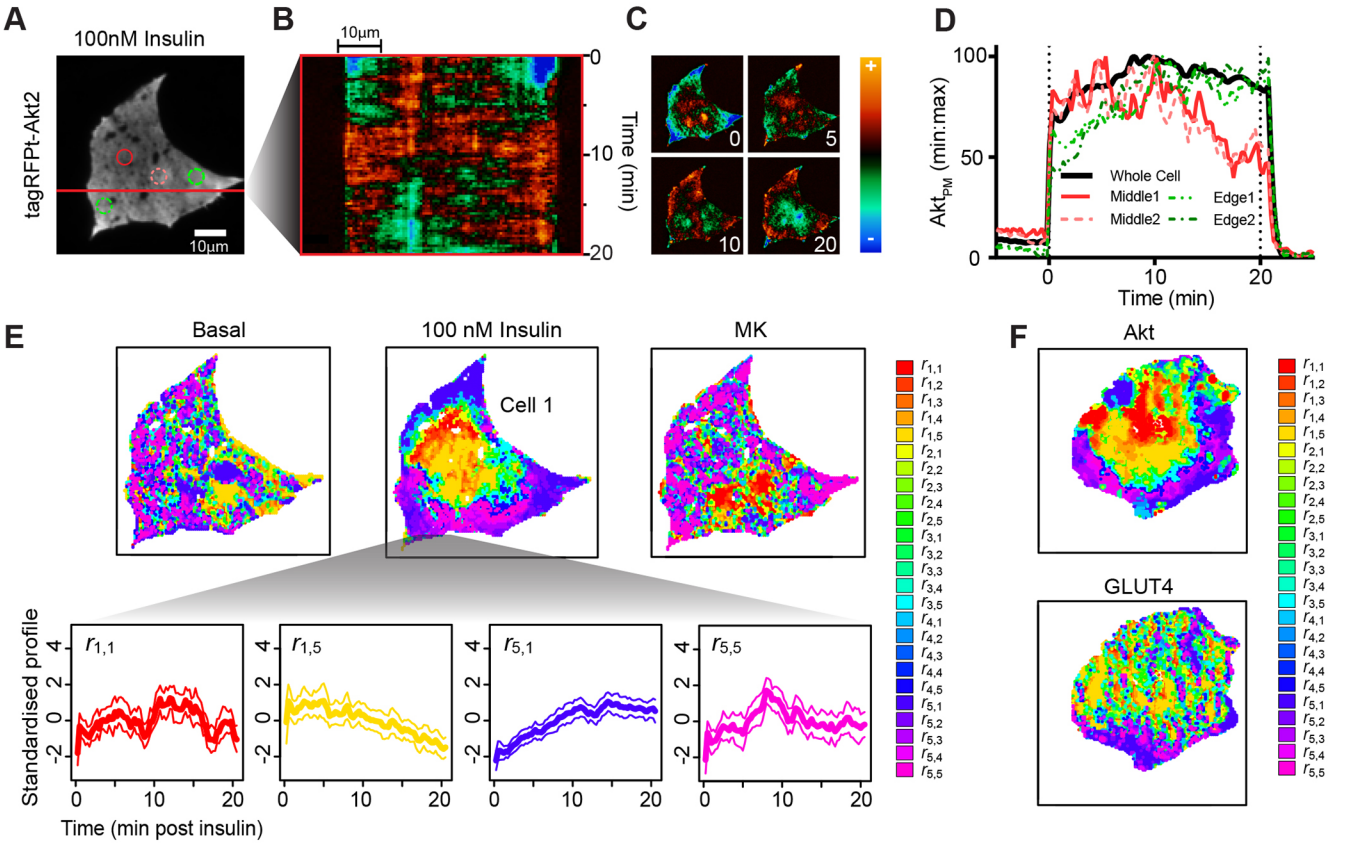

Fig. 3. Insulin stimulates polarised Akt recruitment to the PM. Live 3T3-L1 adipocytes expressing TagRFP-T–Akt2 were imaged by TIRF microscopy. Cells were imaged for 10 min prior to stimulation with 100 nM insulin for 20 min. This was followed by the addition of 10 µM MK2206 (MK). (A) Representative image of a single cell imaged by TIRF microscopy. The red line indicates the plane of the kymograph (B) displayed for 100 nM only. Each pixel has been normalised to the pixel mean across the 100 nM stimulus. (C) Single frames at time points indicated during the 100 nM stimulus response from the same cell as in A and B. (D) Time course of Akt recruitment to the PM for the whole cell and sub-regions demarcated in A. (E) Self-organising map (SOM) analysis results for the same cell that was unstimulated, stimulated with 100 nM insulin or inhibited with MK2206. Colours indicate a clustered response. Panels below show examples of the cluster profiles. (F) SOM analysis applied to a cell co-expressing TagRFP-T–Akt2 and pHluorin–GLUT4 and stimulated with insulin, showing the distinct polarisation of Akt but not GLUT4.

In unstimulated adipocytes, or adipocytes incubated with MK2206 (an inhibitor of Akt membrane recruitment), the patterning of TagRFP-T–Akt2 responses appeared random (Fig. 3E). However, in cells stimulated with 100 nM insulin, there were distinct regions of Akt2 behaviour. This was most notable in the difference between Akt2 responses in the central region of the basement membrane, where Akt2 showed a rapid increase that slowly tapered off with time, and the periphery, where Akt2 increased with time (Fig. 3E; Fig. S2B). This feature of TagRFP-T–Akt2 behaviour was seen in the majority of cells analysed (Fig. S2A). To determine whether these responses were an artefact of imaging or changes in membrane geometry, we next tested whether we observed similar clustering for GLUT4 using the pH-sensitive reporter GLUT4–pHluorin (Burchfield et al., 2013). GLUT4 (also known as SLC2A4) translocates to the PM upon insulin stimulation and acts as a membrane reference under these conditions. When we assessed the clustering patterns of GLUT4 and Akt behaviour in cells co-expressing GLUT4–pHluorin and TagRFP-T–Akt2 following a 100 nM insulin stimulus, the Akt2 responses maintained this grouping of activity described above (Fig. 3E; Fig. S3A), whilst the GLUT4 responses were more random (Fig. 3F; Fig. S3A). GLUT4 responses were similarly random in cells co-expressing GLUT4–TagRFP-T and eGFP–Akt2, however the Akt2 clustering was not evident with the eGFP tag (Fig. S3B). These data support the concept that the clustering pattern of Akt2 membrane translocation observed with TagRFP-T–Akt2 is a bona fide feature of Akt responses to insulin stimulation.

Insulin stimulation induces self-organising oscillations in plasma membrane-associated Akt

Signal transduction pathways utilise temporal signalling patterns, such as oscillations, to encode information of a greater complexity, with enhanced specificity for downstream substrates and processes (Cheong and Levchenko, 2010; Kubota et al., 2012). Self-organising oscillatory behaviour in PIP3 generation, facilitated by PI3K, has been described for amoeboid cells expressing the PH domain of Akt during random cell migration (Arai et al., 2010); however, such oscillations have not yet been demonstrated in response to insulin. Imaging of TagRFP-T–Akt2 in response to insulin in 3T3-L1 adipocytes revealed oscillations in PM Akt that appeared to propagate throughout the cell (Fig. 4A). We applied locally weighted scatterplot smoothing (LOESS)-based normalisation to extract oscillations from individual pixels. The optimal flexibility (span) of the LOESS model was determined by the average of spans selected by Akaike information criterion (AIC) for individual pixels from all cells. This optimal span was then used for subsequent data analysis (Fig. 4B).

Journal of Cell Science (2017) 130, 2757-2766 doi:10.1242/jcs.205369

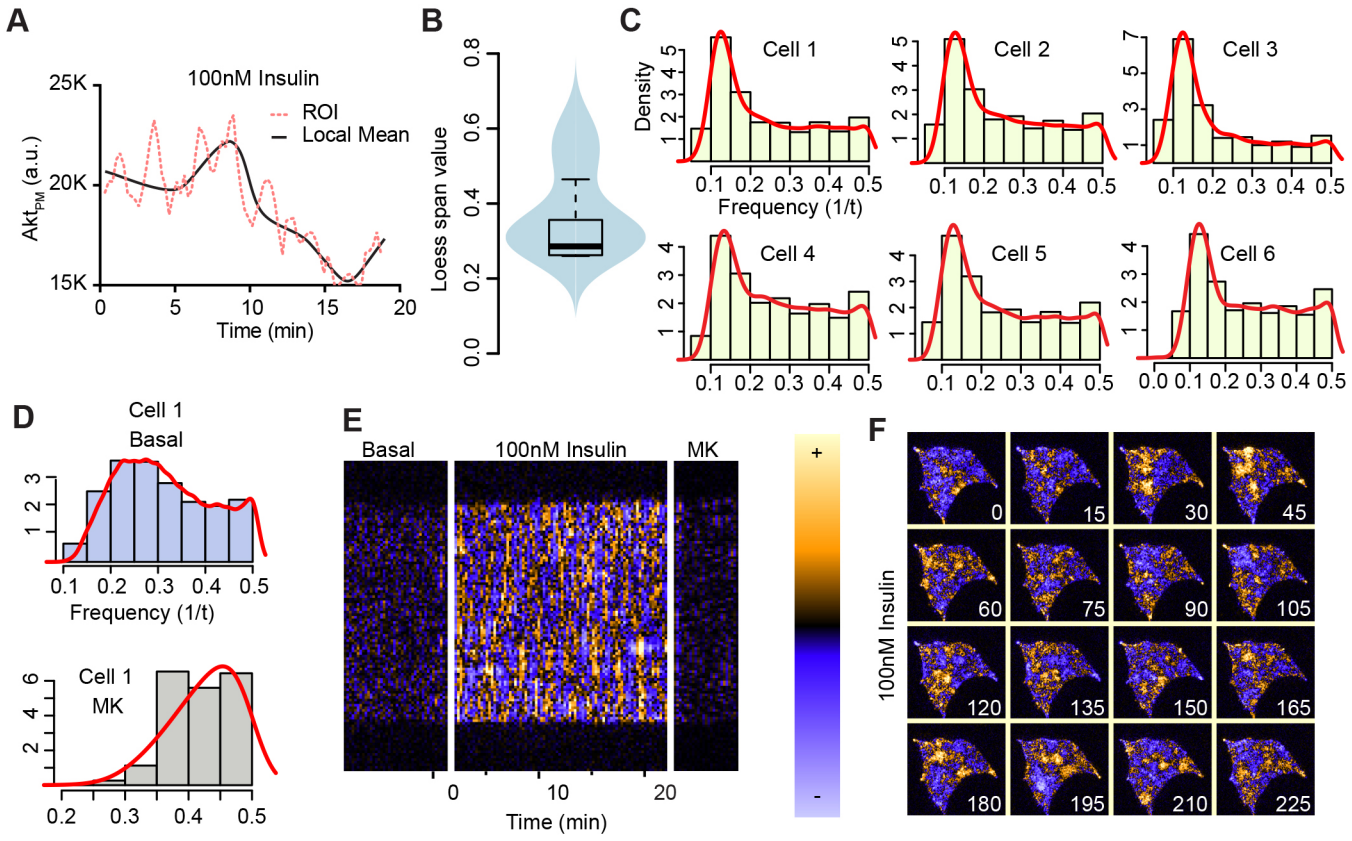

Fig. 4. Insulin-stimulation induces self-organising oscillations in plasma membrane-associated Akt. (A) Oscillations in PM Akt for a 1 μm^2 region of a cell (see Fig. 3A) after 100 nM insulin stimulation, relative to the local mean. (B) Violin plot showing distribution and density of LOESS spans selected for individual pixels based on Akaike information criterion (AIC). The median value of LOESS spans selected for individual pixels was then used as optimal span in the subsequent analysis. The box plot was generated by using the default R base function. (C) Histograms showing the average periodicity of oscillations in individual cells (n=6) in the presence of 100 nM insulin. (D) Histograms of the average periodicity of oscillations in Cell 1 during the basal and MK2206 (MK) periods. (E) Kymograph of a slice of a cell after LOESS normalisation across the entire time course. (F) Representative images from the same cell demonstrating the self-organising nature of the oscillations of Akt at the membrane in response to 100 nM insulin, whereby a given pixel is typically part of a greater similar region, which continues to propagate stochastically across the cell surface.

Single-pixel-resolution periodicities were estimated from each residual profile extracted from the LOESS model through Fourier transformation. These data were plotted on a histogram to identify the average periodicity for each single cell (Fig. 4C,D). In the presence of insulin, the average frequency of oscillations was highly consistent between cells, with a periodicity of ∼2 min (Fig. 4C; Fig. S4A). Distinct reproducible oscillations were not observed in the absence of insulin or in the presence of the Akt inhibitor MK2206, suggesting that the oscillations in PM Akt are a specific feature of insulin signalling (Fig. 4D). The mean amplitude of oscillations varied from cell to cell (Fig. S4B), but did not change within a single cell with respect to time (Fig. S4C). Once established, oscillations were observed to propagate throughout the cell, but the origin of the oscillations and direction of travel appeared to be stochastic (Fig. 4E,F). Although these analyses were carried out at the single-pixel level, the signals at this level were almost always part of a greater region of synchronised oscillations (Fig. 4F). This behaviour is characteristic of a self-organising stochastic process, which is thought to act as a mechanism to facilitate signal plasticity and robustness in response to dynamic perturbations (Kurakin, 2005).

DISCUSSION

Akt is a highly studied kinase that plays a key role cellular signalling and in some disease states, most notably cancer. Here we describe an improved Akt reporter construct, TagRFP-T–Akt2, for monitoring Akt2 localisation in live cells. This new reporter outperformed eGFP–Akt2 in both the magnitude and sensitivity of plasma membrane recruitment in response to insulin in adipocytes. Furthermore, the TagRFP-T–Akt2 construct displayed a dose response that was similar to that of endogenous Akt at the level of insulin-stimulated phosphorylation of Thr309 and Ser474. Imaging of TagRFP-T–Akt2 revealed polarisation of, and specific oscillations in, PM Akt2 in the presence of continuous insulin. These behaviours have not previously been described for Akt in response to insulin and highlight the utility of the TagRFP-T–Akt2 reporter in studying Akt response to growth factors.

At face value, poor recruitment of the eGFP construct suggests that eGFP is interfering with the function of the PH domain. The interaction of Akt with the PM is driven by the interaction between the positively charged PH domain and negatively charged PIP3 (Levental et al., 2008). eGFP has an uneven surface charge distribution that is strongly negative overall. We hypothesised that this charge may result in steric interference with the PH domain via electrostatic attraction or alternatively reduce binding to the PM as a result of electrostatic repulsion. This would explain the diminished recruitment and subsequent phosphorylation of eGFP–Akt2. To test this, we replaced eGFP with the red fluorescent protein TagRFP-T that carries a net neutral surface charge. This change resulted in a dramatic improvement in the ability of the tagged Akt2 construct to

Journal of Cell Science (2017) 130, 2757-2766 doi:10.1242/jcs.205369

bind the PM, supporting the idea that the electrostatic characteristics of eGFP are impeding the function of the PH domain. We cannot, however, discount other mechanisms for the difference between TagRFP-T and eGFP. For example, Ganini and colleagues (Ganini et al., 2017) demonstrated that immature eGFP could produce hydrogen peroxide *in vitro* and that it could activate the oxidative stress response when overexpressed in HeLa cells. TagRFP was shown to produce hydrogen peroxide *in vitro* at a lower rate. It is possible that this may result in oxidation of the PH domain resulting in altered function. The observation that coexpression of TagRFP-T–Akt2 with eGFP–Akt2 did not impair the TagRFP-T–Akt2 response suggests this would need to be an intramolecular phenomenon. Regardless, these data demonstrate that switching the fluorescent protein in fusion constructs can have profound effects on the fidelity of reporters, especially if they undergo localisation changes, and highlight the importance of validating reporters with respect to the endogenous protein.

The TagRFP-T–Akt2 signal-to-noise ratio allowed for the detection of increased PM abundance at a physiological dose of insulin (1 nM, Fig. 1). This is, as far as we are aware, the first report where live-cell and full-length Akt membrane recruitment is visualized through TIRF microscopy in response to a physiologically relevant dose of insulin. Further stimulation with 100 nM resulted in further Akt recruitment in all cells studied, demonstrating that single cells display an intracellular dose response to insulin and that population dose responses are not driven by switch-like behaviour at the single-cell level. These observations of intracellular dose response and intercellular response heterogeneity are consistent with our previous observations (Burchfield et al., 2013), suggesting that differing responses to insulin may be driven by differences in Akt activation.

The increased sensitivity of TagRFP-T–Akt2 revealed new subcellular features of Akt2 membrane recruitment, including both intra-cellular heterogeneity in the Akt2 signal along with the appearance of self-organising oscillations in cell surface Akt2 in the continuous presence of insulin. This behaviour has not been previously reported for Akt in response to insulin. The intensity of the TagRFP-T–Akt2 signal across the plasma membrane in response to insulin was surprisingly variable. The centre of a basal surface of the cell and its periphery displayed markedly distinct response profiles, suggesting that PIP3 production and/or Akt membrane dynamics may be tightly regulated at the subcellular level. In further support of this, we detected oscillations of Akt2 at the membrane, which propagated throughout the cell stochastically. Although this is yet to be described in response to insulin in adipocytes, other groups have reported similar behaviour for the PH domain of Akt, both in MIN6 β-cells in response to glucose and insulin (Hagren and Tengholm, 2006), and in *Dictyostelium* cells during random cell migration (Arai et al., 2010). Although oscillations are potentially a feature of overexpression of a protein which contributes to a feedback loop (Cheong and Levchenko, 2010), the fact that it has been observed in cells expressing just the PH domain of Akt, and thus no kinase functionality, suggests that it is a real phenomenon. Furthermore, the period of the oscillations within single cells was conserved in response to the same stimulus. This may enhance the versatility in the way that Akt, as a central node in a number signalling pathways, processes and transmits signals. The ability to alter periodicity, amplitude, fold-change and duration provides additional layers of information encoded by this signal (Sonnen and Aulehla, 2014) that can then be differentially transmitted to downstream effectors. When assessing the oscillatory patterns, pixels of positive or negative signal are typically part of a much larger area of similar intensity (Fig. 4F). This suggests that the oscillations in membrane Akt localisation are not a random state of disorder, but likely a self-organising behaviour, where Akt molecules synchronise to form a larger functional arrangement. Self-organisation is a process thought to endow systems with adaptability and robustness in response to intra- and extra-cellular changes (De Wolf and Holvoet, 2005; Kurakin, 2005). Given the involvement of Akt in numerous dynamic cellular processes, self-organisation is a likely means by which Akt remains dynamic and sensitive to such stimuli, and the oscillations that arise as a consequence may facilitate signal transmission to specific substrates.

Our studies demonstrate that the choice of fluorophore in generating a fusion construct can have drastic effects on how well this reporter recapitulates properties of the endogenous protein. It is paramount that novel fusion proteins are validated and compared to the endogenous protein of interest in order to generate the most sensitive and informative reporter constructs. Our new TagRFP-T–Akt2 construct accurately reflects the behaviour of endogenous Akt2 and the improvement in sensitivity of TagRFP-T–Akt2 revealed intricate details of Akt membrane recruitment in response to insulin. These features provide insight into the potential mechanisms by which Akt manages and transmits complex signalling information.

MATERIALS AND METHODS

Materials

3T3-L1 murine fibroblasts were sourced from the American Type Culture Collection (ATCC, Manassas, VA) and recently tested and proven to be free of contamination. High glucose Dulbecco's modified Eagle's medium (DMEM), fetal bovine serum (FBS), Glutamax, Trypsin-EDTA, MEM amino acids and FluoroBrite DMEM were from Gibco (11965, 16000-044, 35050, 15400-054, 11130051 and A1896701). 100 mm culture dishes were sourced from Corning (430167) and six-well plates were from Costar (3516). NP40, sodium deoxycholate, SDS, glycerol, sodium orthovanadate, sodium pyrophosphate, ammonium molybdate, dexamethasone, biotin, isobutyl-1-methyl-xanthine (IBMX) and saponin were from Sigma-Aldrich (13021, D6750, L4509, G5516, S6508, S6422, A7302. D4902, B4639, G5516, I5879 and S7900). Glycine was sourced from Univar (1083). Insulin was from Calbiochem. 35 mm glass-bottom dishes were from Ibidi (81158). Matrigel was sourced from Corning (356234). The electroporator used was an ECM 830 Square Wave Electroporation System produced by BTX Molecular Delivery Systems, and the 0.4 cm electroporation cuvettes were sourced from BioRad (16520181). EDTA was sourced from Amresco (0105). Protease inhibitors were from Roche (11873580001) and sodium fluoride was from Fluka (71522). The Pierce Bicinchonic assay kit, Alexa Fluor 488-conjugated goat anti-rabbit SFX and the wheat germ agglutinin–Alexa Fluor 647 conjugate were from ThermoFisher Scientific (23224, A31628 and W32466). Polyvinylidene difluoride membranes were sourced from Merck Millipore (IPVH00010). Antibodies against phosphorylated Akt (pThr308), phosphorylated Akt (pSer473), pan Akt (rabbit), pan Akt (mouse) and phosphorylated AS160 (pThr642) antibodies were sourced from Cell Signalling Technology (9275, 4051, 4685, 2920 and 4288) and the antibody for 14-3-3 was from Santa Cruz Biotechnology (sc-629). All primary antibodies were used at 1:1000 dilution for western blots. For immunofluorescence, primary antibodies were used at 1:100. Paraformaldehyde 16% was sourced from Electron Microscopy Sciences (15710). Dabco 1,4-diazabicyclo(2,2,2) octane was from Polysciences (15154).

Cloning

pDEST53-Cycle3_GFP-Akt2 was cloned using the gateway technique where human Akt2 in the pDONR221 backbone was inserted into pcDNA-DEST53 vector. pDEST53-eGFP-Akt2 was cloned using Gibson assembly from pDEST53-Cycle3_GFP-Akt2 (Gibson et al., 2009). The pDEST53-Akt2 fragment was cloned using the primers 5′-TCTTCGCCCTTAGACACCATGTCTCCCTATAGTGAGTC-3′ and

Journal of Cell Science (2017) 130, 2757-2766 doi:10.1242/jcs.205369

5′-TAATGGCATGGACGAGCTGTACAAGAATGAGGTGTCTGTCAT-CAAAG-3′. The eGFP fragment was cloned from pEGFP-C1 (Clonetech) using the primers 5′-CCAAGCTGGCTAGACACCATGGTGAGCAAG-GGCGAGGA-3′ and 5′-CTTTGATGACAGACACCTCATTCTTGTAC-AGCTCGTCCATGCCATTA-3′.

TagRFP-T–Akt2 was cloned by using Gibson assembly from pDEST53-eGFP-Akt2. The pDEST53-Akt2 fragment was cloned using the same primers as above. The TagRFP-T fragment was cloned from pGEM-T-TagRFP-T using the primers 5′-GACTCACTATAGGGAGAC-ATGGTGTCTAAGGGCGAAGA-3′ and 5′-CTTTGATGACAGACACC-TCATTCTTGTACAGCTCGTCCATGCCATTA-3′.

Preparation of Matrigel-coated dishes

Pipettes were pre-chilled, and Matrigel was diluted 1:50, with sterile ice-cold PBS. Six-well plates and 35 mm glass bottom dishes were coated with the diluted Matrigel and then incubated for 2 h at room temperature. The dishes were then washed twice with room temperature PBS prior to use.

Cell culture and electroporation

3T3-L1 fibroblasts were cultured in DMEM, with 10% FBS and Glutamax at 37°C and 10% CO_2 in 100 mm dishes. Each confluent 100 mm dish of fibroblasts was then reseeded into six-well plates and then differentiated 5 days post seeding in the culture medium described above, supplemented with 0.22 µM dexamethasone, 100 ng/ml biotin, 2 µg/ml insulin and 500 µM IBMX for 3 days. Differentiation medium was then replaced with post-differentiation medium, which is made up of culture medium and 2 µg/ml insulin for a further 3 days. Adipocytes were then refreshed daily with culture medium. At 7 days post differentiation, adipocytes were tryspinised with 5× trypsin-EDTA for 5–10 min at 37°C. Trypsin was quenched with the addition of culture medium, and the cells were centrifuged at 150 ***g*** for 5 min and then washed with PBS and centrifuged twice more. The cell pellet was then resuspended in electroporation solution (20 mM Hepes, 135 mM KCl, 2 mM $MgCl_2$, 0.5% Ficol 400, 1% DMSO, 2 mM ATP and 5 mM glutathione, pH 7.6) and 5–10 µg of plasmid DNA. Cells were then electroporated at 200 mV for 20 ms and then plated onto 35 mm glass-bottom dishes for imaging, or six-well plates coated with Matrigel. Western blot analysis and imaging experiments were performed either 24 or 48 h post electroporation.

Western blotting analysis

48 h after electroporation, adipocytes were serum starved for 2 h at 37°C with 10% CO_2 and then stimulated with either 1 nM or 100 nM insulin. Cells were placed in an ice-cold bath of PBS, then harvested on ice using 400 µl radio-immunoprecipitation assay (RIPA) buffer [50 mM Tris-HCl pH 7.5 (neutralised with NaOH), 150 mM NaCl, 1% NP40, 0.5% sodium deoxycholate, 0.1% SDS, 1 mM EDTA, 1% glycerol] containing phosphatase inhibitors (2 mM sodium orthovanadate, 1 mM sodium pyrophosphate, 1 mM ammonium molybdate and 10 mM sodium fluoride) and protease inhibitors. Lysates were scraped and isolated in 1.5 ml tubes, then sonicated for 15 s, for 1 s on 1 s off. Lysates were centrifuged at 21,000 ***g*** for 30 min to separate insoluble material (lipids and nuclear content). The milky lipid suspension was carefully removed and the supernatant was transferred to a new tube. Protein concentrations were assessed by the bicinchoninic acid method. Lysates were then separated by SDS-PAGE and transferred onto PVDF membranes. Membranes were blocked in 0.5% skimmed milk powder in Tris-buffered saline and 0.1% Tween (TBST) and subsequently blotted for 14-3-3 proteins, phosphorylated Akt (pThr308 and pSer473), pan-Akt (total Akt) and phosphorylated AS160 (pThr642).

Live-cell microscopy

For live experiments, cells were serum-starved in FluoroBrite DMEM (with 0.2% BSA and Glutamax) for 2 h at 37°C with 10% CO_2 and then stimulated with 1 nM and/or 100 nM insulin. For TIRF microscopy, experiments were performed on a Nikon Ti-Lapps H-TIRF module, equipped with an Okolab cage incubator and temperature control. For spinning disk confocal microscopy, experiments were performed on a Nikon Ti-Lapps spinning disk confocal equipped with an Okolab cage incubator and temperature control. Insulin and drugs were added by using a custom-made perfusion system. The system was benchmarked by testing the delivery of 3 ng/ml FITC and 100 ng/ml Alexa Fluor 647-labelled goat anti-rabbit F(ab')2 antibody, to mimic the delivery of drugs and large proteins, respectively. Delivery to the edge and middle of the cell membrane was measured by TIRF. No difference in the delivery to the edge or middle of cells was detected (Fig. S1A).

Immunofluorescence

Cells were seeded into eight-well Ibidi u-slides that had been coated with Matrigel, at day 7 post differentiation. Cells were then allowed to attach for 2 days. On day 9 post differentiation, cells were serum-starved in DMEM (with 0.2% BSA and Glutamax) for 2 h at 37°C with 10% CO_2 and then stimulated with 100 nM insulin. The coverslips were then briefly immersed in an ice-cold PBS bath and instantly fixed with 4% paraformaldehyde at room temperature for 15 min. Cells were then washed twice with room temperature PBS and quenched with 100 mM glycine for 10 min. We then washed the cells twice more with room temperature PBS, and incubated them in blocking and permeabilising buffer (PBS with 2% BSA and 0.1% saponin) for 30 min. Cells were incubated with the anti-pan-Akt (mouse) primary antibody (1:100) overnight at 4°C. The following day, the cells were washed with blocking and permeabilising buffer five times, and then incubated with anti-mouse-IgG conjugated to Alexa Fluor 488 (1:500) at room temperature for 30 min in the dark. Cells were washed five more times with PBS and then stored and imaged in PBS, 5% glycerol and 2.5% Dabco.

Calculation of electrostatic potential

Structure preparation and pK_a calculations were performed for eGFP (PDB 2Y0G), TagRFP-T (PDB 5JVA) and the PH domain of Akt2 (PDB 1P6S) using the PDB2PQR webserver (Dolinsky et al., 2004). Default parameters were used (PARSE forcefield, PH7.0). The Poisson–Boltzmann equation was solved using the adaptive Poisson-Boltzmann solver (APBS) webserver (Baker et al., 2001). The +1 and −1 ion species were set to 150 mM to prevent exaggerated electrostatic properties. Structures and electrostatic maps were visualised with the PyMOL Molecular Graphics System, Version 1.8 Schrödinger, LLC.

Image analysis

Image and statistical analyses were performed using custom analysis pipelines developed in FIJI (Schindelin et al., 2012) and R programming environment.

Temporal signal extraction and characterisation

Distinct molecular (e.g. Akt and GLUT4) recruitment patterns in single cells following various treatments (e.g. basal, insulin and MK2206) were extracted using self-organising maps (SOMs) (Kohonen, 1982), an unsupervised learning procedure that constructs an artificial neural network to scale image data from multi-dimensional space to a two-dimensional space. SOMs not only can characterise pixels based on their temporal signal patterns but also preserve the topological properties of the relative location of individual pixels in a cell image, which is ideal for visualising the temporal and topological inter-relationships in a single cell. Specifically, for each cell, data were standardised to be unit free before feeding into an SOM with a 5-by-5 hexagonal grid denoted as $r_{i,j}$ (i=1…5, j=1…5). Each 'neuron' m_k is updated by an input data point x_t as follows:

$$m_k \leftarrow m_k + \alpha h(||\ell_t - \ell_k||)(x_t - m_k),$$

where α is the learning rate, ℓ is an index to a grid position, and h is a neighbourhood function that assigns more weight to update neuron when it is closer to the input x_t. In our case, we used the Euclidean distance in h to measure the neighbourhood. Individual temporal patterns identified by SOMs from each cell were visualised as bounded line plots by calculating the mean profile of all pixels partitioned in each group and their variance as bounds. Only pixels with signal present for the duration of the time

course were included in this analysis. Thus, any changes in cell, size or shape resulting from insulin stimulation do not influence the analysis.

Oscillation analysis

To extract the oscillation signal, we fitted a locally weighted scatterplot smoothing (LOESS) model (Cleveland and Devlin, 1988) to each individual pixel. The estimated coefficients of LOESS for the ith point at iteration t are found by minimising the following quantity:

$$\sum_{j=1}^{n}(Y_j - (\beta_{0,i}^{(t)} + \beta_{1,i}^{(t)} x_j))^2 \; K_i(x_j),$$

where K is the tricube kernel function and βs are the coefficients estimated for a local the regression line. The optimal span for each LOESS model was determined by Akaike information criterion (AIC) and the average of all optimal spans from all pixels in all cells was used as the final span for subsequent LOESS model fitting. We then extracted the residual matrix from fitted LOESS models for oscillation analysis. Single-pixel-resolution periodicities were estimated from each residual profile extracted from the residual matrix through Fourier transformation, and plotted as histogram to identify the average periodicity for each single cell. We then visualised the oscillation pattern as heatmaps by using the LOESS residual matrix extracted from all pixels in a single cell. To quantify the relative amplitude of oscillation in each cell, for each pixel in a cell, we split its temporal responses extracted from the LOESS fit into non-overlapping windows based on the estimated periodicity in the previous step and calculated the relative amplitude by taking the maximum of absolute values in each window. We then divided this by the average value in that window, giving an amplitude estimate in form of fold change relative to the average in each window. By applying this approach to all pixels in a cell and summarising its distribution, this allowed us to estimate the amplitude for each cell and compare them across multiple cells. To investigate whether the oscillation amplitude remains constant or changed across time, we calculated the difference of amplitudes estimated from the second to the second-last windows for each pixel in a cell and tested whether the distribution of differences is shifted from 0 by using a Wilcox rank sum test. These two windows were chosen to identify any change of amplitude in early and late time points, but avoiding the potential boundary effect on the first and last windows.

Acknowledgements

We are grateful to Dr Daniel Hesselson (Garvan Institute of Medical Research, Sydney) for providing the pGEM-T-TagRFP-T construct. We acknowledge the facilities and the scientific and technical assistance of the Australian Microscopy & Microanalysis Research Facility at the Australian Centre for Microscopy & Microanalysis at the University of Sydney.

Competing interests

The authors declare no competing or financial interests.

Author contributions

Conceptualization: D.M.N., J.R.K., J.G.B.; Methodology: D.M.N., P.Y., J.G.B.; Validation: D.M.N., P.Y., J.G.B.; Formal analysis: D.M.N., P.Y., J.G.B.; Investigation: D.M.N., J.G.B.; Data curation: D.M.N., P.Y.; Writing - original draft: D.M.N., P.Y., D.J.F., J.G.B.; Writing - review & editing: D.M.N., J.R.K., D.J.F., D.J., J.G.B.; Supervision: J.R.K., D.J., J.G.B.; Project administration: J.G.B.; Funding acquisition: D.J.

Funding

This work is supported by National Health and Medical Research Council (NHMRC) grants [GNT1061122, GNT1086850 and GNT1120201 to D.E.J.], an Australian Postgraduate Award scholarship [to D.N.], an Australian Research Council (ARC) Discovery Early Career Research Award [DE170100759 to P.Y.], an NHMRC Early Career Fellowship [APP1072440 to J.R.K.], an NHMRC Senior Principal Research Fellowship [APP1019680 to D.E.J.] and a Diabetes Australia Research Trust Research Program grant [G190680 to J.G.B. and D.J.F.]. The contents of the published material are solely the responsibility of the authors and do not reflect the views of the NHMRC.

Supplementary information

Supplementary information available online at
http://jcs.biologists.org/lookup/doi/10.1242/jcs.205369.supplemental

References

Alessi, D. R., James, S. R., Downes, C. P., Holmes, A. B., Gaffney, P. R. J., Reese, C. B. and Cohen, P. (1997). Characterization of a 3-phosphoinositide-dependent protein kinase which phosphorylates and activates protein kinase Bα. *Curr. Biol.* **7**, 261-269.

Arai, Y., Shibata, T., Matsuoka, S., Sato, M. J., Yanagida, T. and Ueda, M. (2010). Self-organization of the phosphatidylinositol lipids signaling system for random cell migration. *Proc. Natl. Acad. Sci. USA* **107**, 12399-12404.

Asano, Y., Nagasaki, A. and Uyeda, T. Q. P. (2008). Correlated waves of actin filaments and PIP3 in Dictyostelium cells. *Cell Motil. Cytoskeleton* **65**, 923-934.

Baker, N. A., Sept, D., Joseph, S., Holst, M. J. and McCammon, J. A. (2001). Electrostatics of nanosystems: application to microtubules and the ribosome. *Proc. Natl. Acad. Sci. USA* **98**, 10037-10041.

Burchfield, J. G., Lu, J., Fazakerley, D. J., Tan, S.-X., Ng, Y., Mele, K., Buckley, M. J., Han, W., Hughes, W. E. and James, D. E. (2013). Novel systems for dynamically assessing insulin action in live cells reveals heterogeneity in the insulin response. *Traffic* **14**, 259-273.

Calleja, V., Ameer-Beg, S. M., Vojnovic, B., Woscholski, R., Downward, J. and Larijani, B. (2003). Monitoring conformational changes of proteins in cells by fluorescence lifetime imaging microscopy. *Biochem. J.* **372**, 33-40.

Carpten, J. D., Faber, A. L., Horn, C., Donoho, G. P., Briggs, S. L., Robbins, C. M., Hostetter, G., Boguslawski, S., Moses, T. Y., Savage, S. et al. (2007). A transforming mutation in the pleckstrin homology domain of AKT1 in cancer. *Nature* **448**, 439-444.

Carvalho, E., Eliasson, B., Wesslau, C. and Smith, U. (2000). Impaired phosphorylation and insulin-stimulated translocation to the plasma membrane of protein kinase B/Akt in adipocytes from Type II diabetic subjects. *Diabetologia* **43**, 1107-1115.

Cenni, V., Sirri, A., Riccio, M., Lattanzi, G., Santi, S., de Pol, A., Maraldi, N. M. and Marmiroli, S. (2003). Targeting of the Akt/PKB kinase to the actin skeleton. *Cell. Mol. Life Sci.* **60**, 2710-2720.

Cheong, R. and Levchenko, A. (2010). Oscillatory signaling processes: the how, the why and the where. *Curr. Opin. Genet. Dev.* **20**, 665-669.

Cleveland, W. S. and Devlin, S. J. (1988). Locally weighted regression: an approach to regression analysis by local fitting. *J. Am. Stat. Assoc.* **83**, 596-610.

Cranfill, P. J., Sell, B. R., Baird, M. A., Allen, J. R., Lavagnino, Z., de Gruiter, H. M., Kremers, G.-J., Davidson, M. W., Ustione, A. and Piston, D. W. (2016). Quantitative assessment of fluorescent proteins. *Nat. Methods* **13**, 557-562.

Currie, R. A., Walker, K. S., Gray, A., Deak, M., Casamayor, A., Downes, C. P., Cohen, P., Alessi, D. R. and Lucocq, J. (1999). Role of phosphatidylinositol 3,4,5-trisphosphate in regulating the activity and localization of 3-phosphoinositide-dependent protein kinase-1. *Biochem. J.* **337**, 575-583.

Devgan, V., Rao, M. R. S. and Seshagiri, P. B. (2004). Impact of embryonic expression of enhanced green fluorescent protein on early mouse development. *Biochem. Biophys. Res. Commun.* **313**, 1030-1036.

De Wolf, T. and Holvoet, T. (2005). Emergence Versus Self-Organisation: Different Concepts but Promising When Combined. In *Engineering Self-Organising Systems: Methodologies and Applications* (ed. S. A. Brueckner, G. Di Marzo Serugendo, A. Karageorgos and R. Nagpal), pp. 1-15. Berlin, Heidelberg: Springer Berlin Heidelberg.

Dolinsky, T. J., Nielsen, J. E., McCammon, J. A. and Baker, N. A. (2004). PDB2PQR: an automated pipeline for the setup of Poisson-Boltzmann electrostatics calculations. *Nucleic Acids Res.* **32**, W665-W667.

Du, Y., Zhu, H., Li, D., Wang, L., Zhang, L., Luo, Y., Pan, D. and Huang, M. (2014). Lentiviral-mediated overexpression of Akt1 reduces anoxia-reoxygenation injury in cardiomyocytes. *Cell Biol. Int.* **38**, 488-496.

Dummler, B. and Hemmings, B. A. (2007). Physiological roles of PKB/Akt isoforms in development and disease. *Biochem. Soc. Trans.* **35**, 231-235.

Feng, S., Laketa, V., Stein, F., Rutkowska, A., MacNamara, A., Depner, S., Klingmüller, U., Saez-Rodriguez, J. and Schultz, C. (2014). A rapidly reversible chemical dimerizer system to study lipid signaling in living cells. *Angew. Chem. Int. Ed Engl.* **53**, 6720-6723.

Ganini, D., Leinisch, F., Kumar, A., Jiang, J., Tokar, E. J., Malone, C. C., Petrovich, R. M. and Mason, R. P. (2017). Fluorescent proteins such as eGFP lead to catalytic oxidative stress in cells. *Redox Biol.* **12**, 462-468.

Gibson, D. G., Young, L., Chuang, R.-Y., Venter, J. C., Hutchison, C. A., III and Smith, H. O. (2009). Enzymatic assembly of DNA molecules up to several hundred kilobases. *Nat. Methods* **6**, 343-345.

Gonzalez, E. and McGraw, T. E. (2009). Insulin-modulated Akt subcellular localization determines Akt isoform-specific signaling. *Proc. Natl. Acad. Sci. USA* **106**, 7004-7009.

Goto, H., Yang, B., Petersen, D., Pepper, K. A., Alfaro, P. A., Kohn, D. B. and Reynolds, C. P. (2003). Transduction of green fluorescent protein increased oxidative stress and enhanced sensitivity to cytotoxic drugs in neuroblastoma cell lines. *Mol. Cancer Ther.* **2**, 911-917.

Hagren, O. I. and Tengholm, A. (2006). Glucose and insulin synergistically activate phosphatidylinositol 3-kinase to trigger oscillations of phosphatidylinositol 3,4,5-trisphosphate in beta-cells. *J. Biol. Chem.* **281**, 39121-39127.

Hoehn, K. L., Hohnen-Behrens, C., Cederberg, A., Wu, L. E., Turner, N., Yuasa, T., Ebina, Y. and James, D. E. (2008). IRS1-independent defects define major nodes of insulin resistance. *Cell Metab.* **7**, 421-433.
Huang, D. and Shusta, E. V. (2006). A yeast platform for the production of single-chain antibody-green fluorescent protein fusions. *Appl. Environ. Microbiol.* **72**, 7748-7759.
Huang, W. Y., Aramburu, J., Douglas, P. S. and Izumo, S. (2000). Transgenic expression of green fluorescence protein can cause dilated cardiomyopathy. *Nat. Med.* **6**, 482-483.
Huang, B. X., Akbar, M., Kevala, K. and Kim, H.-Y. (2011). Phosphatidylserine is a critical modulator for Akt activation. *J. Cell Biol.* **192**, 979-992.
Imazaki, A., Tanaka, A., Harimoto, Y., Yamamoto, M., Akimitsu, K., Park, P. and Tsuge, T. (2010). Contribution of peroxisomes to secondary metabolism and pathogenicity in the fungal plant pathogen Alternaria alternata. *Eukaryot. Cell* **9**, 682-694.
Kalatskaya, I., Schüssler, S., Seidl, C., Jochum, M. and Faussner, A. (2006). C-Terminal fusion of eGFP to the bradykinin B2 receptor strongly affects down-regulation but not receptor internalization or signaling. *Biol. Chem.* **387**, 603-610.
Kandel, E. S. and Hay, N. (1999). The regulation and activities of the multifunctional serine/threonine kinase Akt/PKB. *Exp. Cell Res.* **253**, 210-229.
Kohonen, T. (1982). Self-organized formation of topologically correct feature maps. *Biol. Cybern.* **43**, 59-69.
Kontos, C. D., Stauffer, T. P., Yang, W.-P., York, J. D., Huang, L., Blanar, M. A., Meyer, T. and Peters, K. G. (1998). Tyrosine 1101 of Tie2 is the major site of association of p85 and is required for activation of phosphatidylinositol 3-kinase and Akt. *Mol. Cell. Biol.* **18**, 4131-4140.
Kubota, H., Noguchi, R., Toyoshima, Y., Ozaki, Y.-I., Uda, S., Watanabe, K., Ogawa, W. and Kuroda, S. (2012). Temporal coding of insulin action through multiplexing of the AKT pathway. *Mol. Cell* **46**, 820-832.
Kurakin, A. (2005). Self-organization versus Watchmaker: stochastic dynamics of cellular organization. *Biol. Chem.* **386**, 247-254.
Lasserre, R., Guo, X.-J., Conchonaud, F., Hamon, Y., Hawchar, O., Bernard, A.-M., Soudja, S. M., Lenne, P.-F., Rigneault, H., Olive, D. et al. (2008). Raft nanodomains contribute to Akt/PKB plasma membrane recruitment and activation. *Nat. Chem. Biol.* **4**, 538-547.
Levental, I., Janmey, P. A. and Cēbers, A. (2008). Electrostatic contribution to the surface pressure of charged monolayers containing polyphosphoinositides. *Biophys. J.* **95**, 1199-1205.
Liu, H. S., Jan, M. S., Chou, C. K., Chen, P. H. and Ke, N. J. (1999). Is green fluorescent protein toxic to the living cells? *Biochem. Biophys. Res. Commun.* **260**, 712-717.
Manning, B. D. and Cantley, L. C. (2007). AKT/PKB signaling: navigating downstream. *Cell* **129**, 1261-1274.
Mawhinney, R. M. S. and Staveley, B. E. (2011). Expression of GFP can influence aging and climbing ability in Drosophila. *Genet. Mol. Res.* **10**, 494-505.
Ng, Y., Ramm, G., Lopez, J. A. and James, D. E. (2008). Rapid activation of Akt2 is sufficient to stimulate GLUT4 translocation in 3T3-L1 adipocytes. *Cell Metab.* **7**, 348-356.
Parikh, C., Janakiraman, V., Wu, W.-I., Foo, C. K., Kljavin, N. M., Chaudhuri, S., Stawiski, E., Lee, B., Lin, J., Li, H. et al. (2012). Disruption of PH-kinase domain interactions leads to oncogenic activation of AKT in human cancers. *Proc. Natl. Acad. Sci. USA* **109**, 19368-19373.
Rodríguez-Escudero, I., Roelants, F. M., Thorner, J., Nombela, C., Molina, M. and Cid, V. J. (2005). Reconstitution of the mammalian PI3K/PTEN/Akt pathway in yeast. *Biochem. J.* **390**, 613-623.
Sarbassov, D. D. (2005). Phosphorylation and regulation of Akt/PKB by the rictor-mTOR Complex. *Science* **307**, 1098-1101.
Schindelin, J., Arganda-Carreras, I., Frise, E., Kaynig, V., Longair, M., Pietzsch, T., Preibisch, S., Rueden, C., Saalfeld, S., Schmid, B. et al. (2012). Fiji: an open-source platform for biological-image analysis. *Nat. Methods* **9**, 676-682.
Seibel, N. M., Eljouni, J., Nalaskowski, M. M. and Hampe, W. (2007). Nuclear localization of enhanced green fluorescent protein homomultimers. *Anal. Biochem.* **368**, 95-99.
Servant, G., Weiner, O. D., Herzmark, P., Balla, T., Sedat, J. W. and Bourne, H. R. (2000). Polarization of chemoattractant receptor signaling during neutrophil chemotaxis. *Science* **287**, 1037-1040.
Shaner, N. C., Lin, M. Z., McKeown, M. R., Steinbach, P. A., Hazelwood, K. L., Davidson, M. W. and Tsien, R. Y. (2008). Improving the photostability of bright monomeric orange and red fluorescent proteins. *Nat. Methods* **5**, 545-551.
Skube, S. B., Chaverri, J. M. and Goodson, H. V. (2010). Effect of GFP tags on the localization of EB1 and EB1 fragments in vivo. *Cytoskeleton* **67**, 1-12.
Sonnen, K. F. and Aulehla, A. (2014). Dynamic signal encoding—From cells to organisms. *Semin. Cell Dev. Biol.* **34**, 91-98.
Tan, S.-X., Ng, Y., Meoli, C. C., Kumar, A., Khoo, P.-S., Fazakerley, D. J., Junutula, J. R., Vali, S., James, D. E. and Stöckli, J. (2012). Amplification and demultiplexing in insulin-regulated Akt protein kinase pathway in adipocytes. *J. Biol. Chem.* **287**, 6128-63138.
Terashima, Y., Onai, N., Murai, M., Enomoto, M., Poonpiriya, V., Hamada, T., Motomura, K., Suwa, M., Ezaki, T., Haga, T. et al. (2005). Pivotal function for cytoplasmic protein FROUNT in CCR2-mediated monocyte chemotaxis. *Nat. Immunol.* **6**, 827-835.
Wang, Y. (2006). Akt binds to and phosphorylates phospholipase C- γ1 in response to epidermal growth factor. *Mol. Biol. Cell* **17**, 2267-2277.
Wang, R. and Brattain, M. G. (2006). AKT can be activated in the nucleus. *Cell. Signal.* **18**, 1722-1731.
Watton, S. J. and Downward, J. (1999). Akt/PKB localisation and 3' phosphoinositide generation at sites of epithelial cell-matrix and cell-cell interaction. *Curr. Biol.* **9**, 433-436.
Yantsevich, A. V., Gilep, A. A. and Usanov, S. A. (2009). Conformational stability of cytochrome b_5, enhanced green fluorescent protein, and their fusion protein $Hmwb_5$-EGFP. *Biochemistry* **74**, 518-527.
Zhang, F., Hackett, N. R., Lam, G., Cheng, J., Pergolizzi, R., Luo, L., Shmelkov, S. V., Edelberg, J., Crystal, R. G. and Rafii, S. (2003). Green fluorescent protein selectively induces HSP70-mediated up-regulation of COX-2 expression in endothelial cells. *Blood* **102**, 2115-2121.
Zhang, C., Yang, N., Yang, C.-h., Ding, H.-s., Luo, C., Zhang, Y., Wu, M.-j., Zhang, X.-w., Shen, X., Jiang, H.-l. et al. (2009). S9, a novel anticancer agent, exerts its anti-proliferative activity by interfering with both PI3K-Akt-mTOR signaling and microtubule cytoskeleton. *PLoS ONE* **4**, e4881.
Zhu, M., Ni, W., Dong, Y. and Wu, Z.-Y. (2013). EGFP tags affect cellular localization of ATP7B mutants. *CNS Neurosci. Ther.* **19**, 346-351.

Supplementary Figure 1

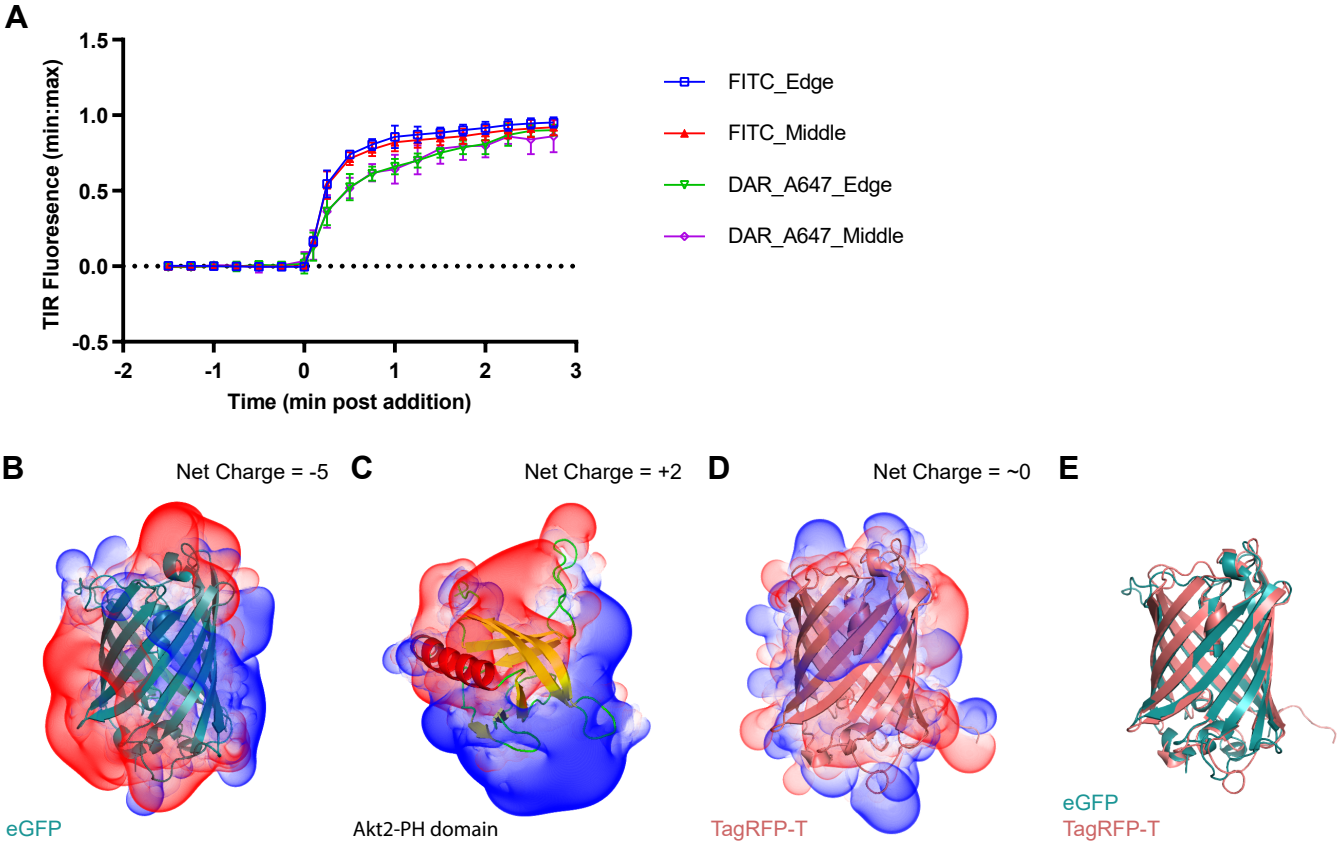

Supplementary Figure 1. (**A**) **Custom perfusion system performance**. Delivery of 3 ng/ml FITC and 100 ng/ml Alexa-647 labelled goat anti-rabbit F(ab')2 antibody to the edge and middle of cells mas measured by TIRF. **eGFP has a strongly negative electrostatic charge, TagRFP-T does not.** (**B**) eGFP, (**C**) the PH domain of Akt2 and (**D**) TagRFP-T overlaid with their respective electrostatic potential calculated using the Adaptive Poisson-Boltzmann Solver (APBS) at 150 mM ionic strength with a solute dielectric of 2 and a solvent dielectric of 78.5 and rendered using PyMOL Volume visualisation. Highly negative regions are displayed as opaque red and highly positive regions as opaque blue. Borders are equivalent to isocontours at +-1 kT/e. (**E**) Aligned cartoon representations of eGFP and TagRFP-T.

Supplementary Figure 2

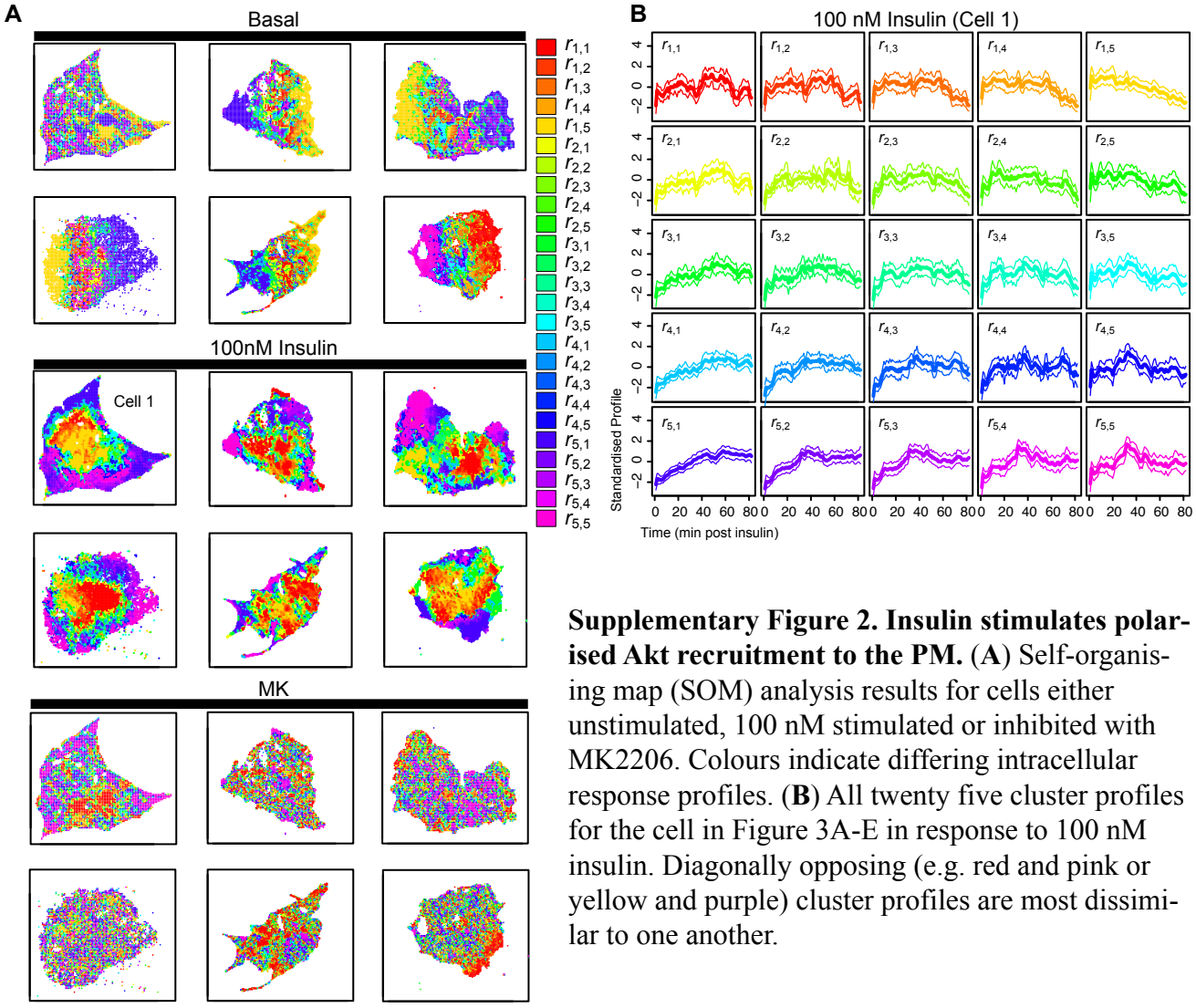

Supplementary Figure 2. Insulin stimulates polarised Akt recruitment to the PM. (**A**) Self-organising map (SOM) analysis results for cells either unstimulated, 100 nM stimulated or inhibited with MK2206. Colours indicate differing intracellular response profiles. (**B**) All twenty five cluster profiles for the cell in Figure 3A-E in response to 100 nM insulin. Diagonally opposing (e.g. red and pink or yellow and purple) cluster profiles are most dissimilar to one another.

Supplementary Figure 3

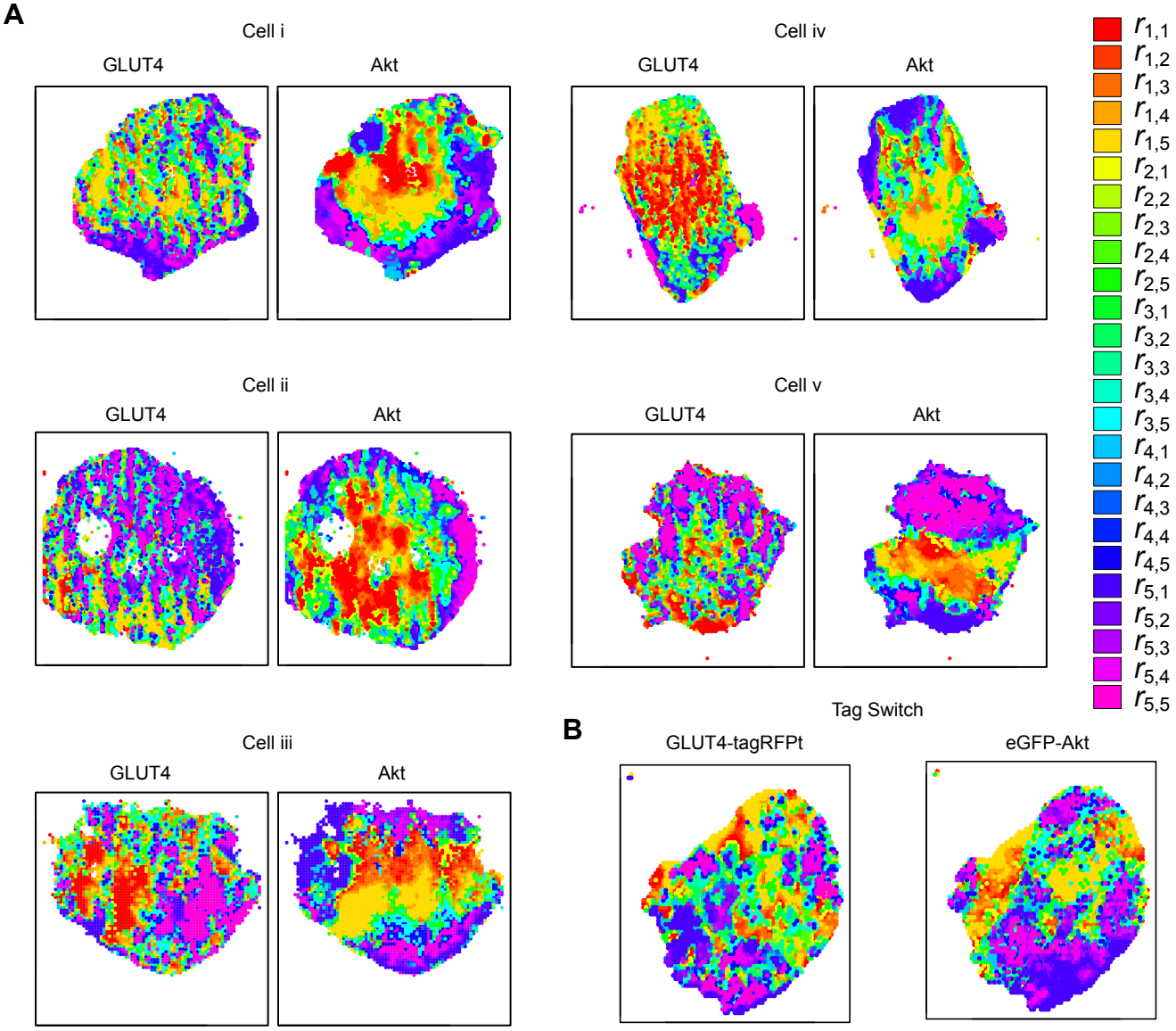

Supplementary Figure 3. Insulin stimulated membrane polarisation is specific for Akt but not GLUT4. (**A**) Self-organising map (SOM) analysis for 5 cells co-expressing GLUT4-pHluorin and TagRFP-T-Akt2 stimulated with 100 nM insulin. (**B**) Self-organising map (SOM) analysis for a cell co-expressing GLUT4-tagRFP-T and eGFP-Akt2 stimulated with 100 nM insulin. Colours indicate differing intracellular response profiles.

Supplementary Figure 4

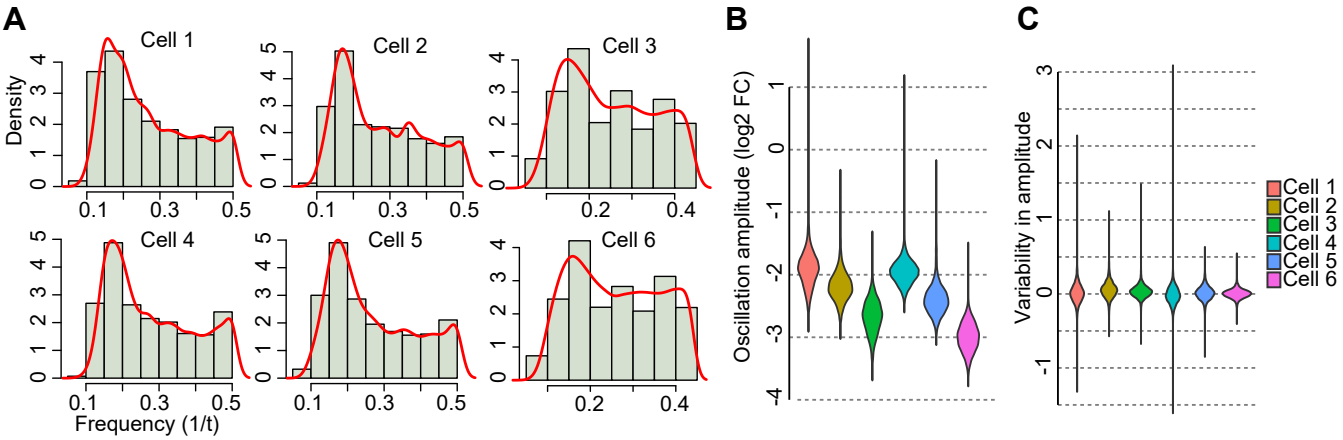

Supplementary Figure 4. Oscillation frequency, but not amplitude, is consistent across multiple cells. (**A**) Comparison of oscillation frequency for six cells in addition to those in Figure 4C (from 2 independent experiments) across a 100 nM insulin-stimulated timecourse. (**B**) Comparison of oscillation amplitude for each individual cell in Figure 4C across the 100 nM-stimulated timecourse. (**C**) Oscillation amplitude variability within each cell across the timecourse.